An anomalous subauroral red arc on 4 August, 1972: comparison of ISIS-2 satellite data with numerical calculations

V. V. Lobzin, A. V. Pavlov, N. M. Pavlova

Institute of Terrestrial Magnetism, Ionosphere and Radio-Wave Propagation, Russian Academy of Science (IZMIRAN), Troitsk, Moscow Region, 142092, Russia
E-mail: pavlov@charley.izmiran.rssi.ru

Abstract. This study compares the Isis II satellite measurements of the electron density and temperature, the integral airglow intensity and volume emission rate at 630 nm in the SAR arc region, observed at dusk on 4 August, 1972, in the Southern Hemisphere, during the main phase of the geomagnetic storm. The model results were obtained using the time dependent one-dimensional mathematical model of the Earth's ionosphere and plasmasphere (the IZMIRAN model). The major enhancement to the IZMIRAN model developed in this study to explain the two component 630 nm emission observed is the analytical yield spectrum approach to calculate the fluxes of precipitating electrons and the additional production rates of N_2^+, O_2^+, $O^+(^4S)$, $O^+(^2D)$, $O^-(^2P)$, and $O^+(^2P)$ ions, and $O(^1D)$ in the SAR arc regions in the Northern and Southern Hemispheres. In order to bring the measured and modelled electron temperatures into agreement, the additional heating electron rate of $1.05\,\mathrm{eV\,cm^{-3}\,s^{-1}}$ was added in the energy balance equation of electrons at altitudes above 5000 km during the main phase of the geomagnetic storm. This additional heating electron rate determines the thermally excited 630 nm emission observed. The IZMIRAN model calculates a 630 nm integral intensity above 350 km of 4.1 kR and a total 630 nm integral intensity of 8.1 kR, values which are slightly lower compared to the observed 4.7 kR and 10.6 kR. We conclude that the 630 nm emission observed can be explained considering both the soft energy electron excited component and the thermally excited component. It is found that the inclusion of $N_2(v>0)$ and $O_2(v>0)$ in the calculations of the $O^+(^4S)$ loss rate improves the agreement between the calculated N_e and the data on 4 August, 1972. The $N_2(v>0)$ and $O_2(v>0)$ effects are enough to explain the electron density depression in the SAR arc F-region and above F2 peak altitude. Our calculations show that the increase in the $O^+ + N_2$ rate factor due to the vibratio-

nally excited nitrogen produces the 5–19% reductions in the calculated quiet daytime peak density and the 16–24% decrease in NmF2 in the SAR arc region. The increase in the $O^+ + N_2$ loss rate due to vibrationally excited O_2 produces the 7–26% decrease in the calculated quiet daytime peak density and the 12–26% decrease in NmF2 in the SAR arc region. We evaluated the role of the electron cooling rates by low-lying electronic excitation of $O_2(a^1\Delta_g)$ and $O_2(b^1\Sigma_g^+)$, and rotational excitation of O_2, and found that the effect of these cooling rates on T_e can be considered negligible during the quiet and geomagnetic storm period 3–4 August, 1972. The energy exchange between electron and ion gases, the cooling rate in collisions of $O(^3P)$ with thermal electrons with excitation of $O(^1D)$, and the electron cooling rates by vibrational excitation of O_2 and N_2 are the largest cooling rates above 200 km in the SAR arc region on 4 August, 1972. The enhanced IZMIRAN model calculates also number densities of $N_2(B^3\Pi_g^+)$, $N_2(C^3\Pi_u)$, and $N_2(A^3\Sigma_u^+)$ at several vibrational levels, $O(^1S)$, and the volume emission rate and integral intensity at 557.7 nm in the region between 120 and 1000 km. We found from the model that the integral intensity at 557.7 nm is much less than the integral intensity at 630 nm.

1 Introduction

The characteristic spectral emissions at 630 nm that identify stable auroral red (SAR) arcs are observed optically on the equatorward edge of the mid-latitude ionospheric trough in both the Northern and Southern Hemispheres on approximately the same L shell value of

Correspondence to: A. V. Pavlov

the geomagnetic field during large magnetic storms characterised by geomagnetic planetary index K_p of 5 or greater (Rees and Roble, 1975; Kozyra *et al.*, 1997). A major part of ground and satellite observations that determine the properties of the SAR arcs have been obtained in the Northern Hemisphere. The observed SAR arc properties in magnetically conjugate hemispheres were discussed only by Reed and Blamont (1968), who determined the positions of the SAR arcs on 28–29 September, 1967, using data from the satellite Ogo 4, and LaValle and Elliot (1972), who presented and discussed OV1-10 satellite data on 16 February, 1967, and Pavlov (1997), who studied the SAR arcs measured by the OV1-10 photometer on 16 February, 1967. We present the results of the first calculations and studies of the SAR arc in the Southern Hemisphere observed at dusk on 4 August, 1972 (Shepherd *et al.*, 1980).

Unusual SAR arc features observed at dusk on 4 August, 1972 in the Southern Hemisphere may be stated as follows:

1. Very high measured integral intensity at 630 nm (up to 10.6 kR) was registered.

2. SAR arcs are usually observed during recovery phase of large magnetic storms (Rees and Roble, 1975; Kozyra *et al.*, 1997) while the studied SAR arc event was observed during the main phase of the magnetic storm.

3. SAR arcs are associated with the atomic oxygen transition $OI(^3P_2\text{-}^1D_2)$. As a rule, the production rate of $O(^1D)$ arising from the collisions of thermal electrons with $O(^3P)$ is enough to explain the measured intensities (Rees and Roble, 1975; Kozyra *et al.*, 1997). However, for some SAR arcs the resultant model intensities are much less than the measured intensities and this suggests that an additional $O(^1D)$ source associated with precipitation component to SAR arc generation by soft electrons may have been present in these SAR arcs (Prasad *et al.*, 1980; Gurgiolo *et al.*, 1982; Slater *et al.*, 1987; Foster *et al.*, 1994; Kozyra *et al.*, 1997). Of special interest to this work, the studied 630 nm emission can be divided into two components excited by thermal electrons and low energy precipitating electrons (Shepherd *et al.*, 1980).

In the present study an attempt is made to model this anomalous SAR arc and illustrate the basic physics involved.

Observations of the subauroral ionosphere have confirmed that at F-region altitudes within the SAR arc the electron density is reduced and the electron temperature, T_e, is enhanced compared with the region outside the arc (Rees and Roble, 1975; Kozyra *et al.*, 1997). It has been shown that the loss of oxygen ions due to interactions with vibrationally excited nitrogen, according to the reaction

$$O^+(^4S) + N_2(v > 0) \rightarrow NO^+ + N \ , \tag{1}$$
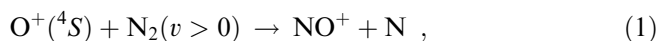
where v indicates the vibrational level, is increased in SAR arc region as a result of the increased excitation of nitrogen vibrational levels by collisions with the hot thermal electrons (Newton *et al.*, 1974; Pavlov, 1989;

Pavlov and Namgaladze, 1988). Nevertheless, Maier *et al.* (1975), Newton and Walker (1975), and Raitt *et al.* (1976) have concluded that this increase in the loss rate of $O^+(^4S)$ as a result of the increase in the N_2 vibrational temperature does not produce enough of an effect on electron density to explain the observed density decrease. However, Pavlov (1996) found that the loss rate of $O^+(^4S)$ due to reaction (1) is enough to explain the factor of 2 electron density depression at F-region heights and the topside ionosphere density variations within the SAR arc observed on 18 December, 1971.

The measurements of the effective rate coefficient for the reaction of $O^+(^4S)$ with N_2 was given by Hierl *et al.* (1997) over the temperature range 300–1600 K for $T_n = T_i = T_v$, where T_n is the neutral temperature, T_i is the ion temperature, and T_v is the vibrational temperature of N_2. These results confirm the observations of Schmeltekopf *et al.* (1968) and show that the assumption of similar translation temperature dependencies for different vibrational states of N_2 is reasonable. The model used in this study is the IZMIRAN time-dependent mathematical model of the Earth's ionosphere and plasmasphere (Pavlov, 1997, 1998b) using the results of Hierl *et al.* (1997). Such an approach gives an opportunity to study the role of $N_2(v)$ in the formation of the electron density depression in the SAR arc region.

The important chemical processes in determining the abundance of $O^+(^4S)$ ions are also the reaction

$$O^+(^4S) + O_2(v) \rightarrow O_2^+ + O \ , \tag{2}$$
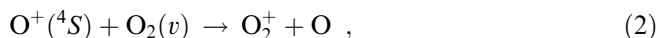
where $v = 0, 1, \ldots$ is the number of vibrational level of O_2.

Hierl *et al.* (1997) found a big difference between the high temperature flowing afterglow and drift tube measurements (McFarland *et al.*, 1973; Albritton *et al.*, 1977) of the effective rate coefficient for the reaction $O^+(^4S)$ with O_2 as a result of the input of the reactions between the vibrationally excited O_2 and $O^+(^4S)$ over the temperature range 300–1800 K for $T_n = T_i = T_{vib}$, where T_{vib} is the vibrational temperature of O_2. Using the flowing afterglow measurements of the effective rate coefficient for the reactions of $O^+(^4S)$ with O_2 given by Hierl *et al.* (1997), Pavlov (1998b) evaluated the approximate contribution of each vibrational state of $O_2(v)$ and found the partial rate coefficients for vibrational quantum number $v = 1$–5 which can be used in calculations of electron densities. These new results will be used here to evaluate for the first time the role of $O_2(v)$ in the SAR arc region.

2 Theoretical model

The model used is the IZMIRAN model that we have steadily developed over the years (Pavlov, 1997, 1998b). The chemistry, physics, and solution procedure have been described in details by Pavlov (1997, 1998b), and hence only a brief description of the IZMIRAN model is given. It is a one-dimensional model that uses a tilted dipole approximation to the Earth's magnetic field and takes into account the offset between the geographic and

geomagnetic axes. In the model, coupled time dependent equations of continuity and energy balance, and diffusion equations for electrons, and $O^+(^4S)$, H^+, and He^+ ions are solved along a centred-dipole magnetic field line for the concentrations, temperatures, and field-aligned diffusion velocities of ions and electrons from a base altitude (160 km) in the Northern Hemisphere through the plasmasphere to the same base altitude in the Southern Hemisphere. Electron heating due to photoelectrons is provided by a solution of the Boltzmann equation for photoelectron flux. In the altitude range 120–700 km in the Northern and Southern Hemispheres the IZMIRAN model solves time-dependent continuity equations for $O^+(^2D)$, $O(^2P)$, NO^+, O_2^+, N_2^+, and vibrationally excited molecular nitrogen, $N_2(v)$ and oxygen, $O_2(v)$, at the first five vibrational levels $v = 1$–5. $O^+(^4P)$ and $O^+(^2P^*)$ ions are also included in the IZMIRAN model as described by Pavlov (1998b). The diffusion of ions and excited species are taken into account in continuity equations for NO^+, O_2^+, $O_2(v)$, and $N_2(v)$. As a consequence of the large rate coefficients for chemical reactions of metastable $O^+(^2D)$ and $O^+(^2P)$ ions with neutrals in comparison with those for $O^+(^4S)$ ions (see Table 1 of Pavlov, 1997), the loss rate of these metastable ions is higher than the loss rate of unexcited $O^+(^4S)$ ions by a factor of 100–1000 while the characteristic diffusion time is the same. As a result, the role of the $O^+(^2D)$ and $O^+(^2P)$ diffusion is negligible in comparison with the role for chemical reactions for these metastable ions and the $O^+(^2D)$ and $O^+(^2P)$ diffusion is not considered in calculations of $[O^+(^2D)]$ and $[O^+(^2P)]$ (Torr and Torr, 1982). The chemical reactions with their rate coefficients are presented in Table 1 of Pavlov (1997) for $O^+(^4S)$, H^+, He^+, $O^+(^2D)$, $O^+(^2P)$, NO^+, O_2^+, N_2^+ ions. The IZMIRAN model uses the recombination rate coefficient of $O^+(^4S)$ ions with unexcited $N_2(0)$ and $O_2(0)$ and vibrationally excited $N_2(v)$ and $O_2(v)$ as described in detail by Pavlov (1998b). The continuity and energy equations for the vibrationally excited N_2 and O_2 are described by Pavlov (1997, 1998b). We use the revised electron cooling rates by vibrational and rotational excitation of O_2 and N_2 of Pavlov (1998a, c). The new analytical expression for atomic oxygen fine structure cooling rate of thermal electrons of Pavlov and Berrington (1999) based on the $O(^3P)$ excitation cross sections of Bell et al. (1998) is included in the updated IZMIRAN model.

To calculate the density of NO the model given by Titheridge (1997) is used. We have no information on the peak altitude, hmF2, and thus can use neither the method developed by Richards (1991) nor our modification of it (Pavlov and Buonsanto, 1997) to calculate an equivalent plasma drift velocity. To overcome this problem, we use our approach described by Pavlov (1996, 1997) which allows us to avoid some serious errors in the calculations of hmF2 during magnetic storms (Pavlov and Buonsanto, 1997).

The updated IZMIRAN model includes the analytical yield spectrum approach developed by Green et al. (1977), Jackman and Green (1979), Singhal et al. (1979), Singhal and Green (1981), and Haider and Singhal (1983) to calculate the fluxes of precipitating electrons in the altitude range 120–1000 km of Northern and Southern Hemispheres if an incident electron flux is given at the upper boundary. The validity of this approach is corroborated by the comparison of the calculated fluxes of precipitating electrons in the energy range 2 eV–10 keV and volume excitation and ionization rates from the analytical yield spectrum approach with those from Banks et al. (1974) and Mantas and Walker (1974) (see Haider and Singhal, 1983). Our implementation of this analytical method is explained in the Appendix. The electron-impact ionization cross sections of N_2 and O_2 are taken from Hwang et al. (1996) to calculate the additional production rates of N_2^+ and O_2^+ ions in the SAR arc regions due to fluxes of precipitating electrons. The cross sections of Laher and Gilmore (1990) for electron-impact ionization of atomic oxygen are used to form $O^+(^4S)$, $O^+(^2D)$, $O^+(^2P)$, and $O^+(^2P)$ ions. To calculate the additional production rate of $O(^1D)$ due to precipitating electrons the excitation cross section for the $O(^3P \rightarrow {}^1D)$ transition, given by Doering (1992), is used.

The IZMIRAN model calculates $[O(^1D)]$ from a time-dependent continuity equation in the region between 120 and 1500 km in altitude using production of $O(^1D)$ by photodissociation of oxygen molecules, $O(^1D)$ formation by collisions between $O(^3P)$ and thermal electrons, precipitating electrons and photoelectrons, diffusion of $O(^1D)$ through mixture of $N_2(0)$, O_2, and O, chemical reactions of $O(^1D)$ with N_2, O_2, O, and electrons, and atomic oxygen transitions $O(^1D) \rightarrow O(^3P_2) + h\nu$ at 630 nm, $O(^1D) \rightarrow O(^3P_1) + h\nu$ at 636.4 nm, $O(^1D) \rightarrow O(^3P_0) + h\nu$ at 639.1 nm with rate and diffusion coefficients given by Pavlov (1997) (see Eqs. A24, A25, and Table 3 of Pavlov 1997). In this study we use the Einstein coefficient $A_{630} = 5.61 \cdot 10^{-3}\,\text{s}^{-1}$ given by Bhatia and Kastner (1995) instead of $A_{630} = 5.63 \cdot 10^{-3}\,\text{s}^{-1}$ used by Pavlov (1997). The Einstein coefficients $A_{636.4} = 1.82 \cdot 10^{-3}\,\text{s}^{-1}$ and $A_{639.1} = 8.92 \cdot 10^{-7}\,\text{s}^{-1}$ recommended by Bhatia and Kastner (1995) are the same as used by Pavlov (1997).

The production and loss rate of $O(^1D)$ arising from the collisions of thermal electrons with $O(^3P)$ includes both excitation and deexcitation of $O(^1D)$ and can be calculated as (Stubbe and Varnum, 1972)

$$P_t = N_e\, f(T_e)\{[O] - [O(^1D)]g_1 g_0^{-1} \exp(E_0/T_e)\}\,, \qquad (3)$$

where $f(T_e) = \{8k\,T_e(\pi\,m_e)^{-1}\}^{0.5}\int_0^\infty \sigma(x)x\exp(-x)dx$, $x = E(kT_e)^{-1}$, $\sigma(E)$ is the cross section for excitation of the $O(^1D)$ state by electrons, E is the energy of electrons, k is the Boltzmann constant, m_e denotes the mass of electron, g_0, and g_1 are statistical weights of the electron levels ^3P, and ^1D of O, $g_1 g_0^{-1} = 1.8$ (Radzig and Smirnov, 1980), and $E_0 = 22829\,\text{K}$ (or 1.97 eV) is the energy of the $O(^1D)$ electron level given by Radzig and Smirnov (1980).

The analytical formula for $f(T_e)$ which was used in the IZMIRAN model was based on $\sigma(E) = \sigma_0 E_0(1 - E_0/E)^2/E$ where the value of σ_0 was determined by fitting this $\sigma(E)$ to the measured (Doering and Gulcicek, 1989) and theoretical (Thomas and Nesbet,

1975) cross sections (Pavlov, 1996; 1997). The value of $\sigma(E)$ has been measured by Doering (1992) for incident electron impact energies of 4.0 to 30 eV. To find a more accurate analytical expression for $f(T_e)$ we used the linear interpolation of $\sigma(E)$ measured by Doering (1992) between fixed incident energies from the threshold (where $\sigma(E) = 0$) to 30 eV. This assumption leads to the simple approach in calculations of $f(T_e)$ as

$$f(T_e) = 4.71 \cdot 10^{-12} \, T_e^{0.7} (1 + 6.25 \cdot 10^{-10} \, T_e^2) \exp(-E_0/T_e) , \tag{4}$$

where the unit of $f(T_e)$ is $cm^3 \, s^{-1}$.

We found that the value of maximum error for this analytical expression for $f(T_e)$ is less than 2% within the electron temperature range 1300–8000 K, and this accuracy is enough for our studies. It should be noted that the difference between the new and old IZMIRAN model values of $f(T_e)$ is less than 10% within the electron temperature range 2500–8000 K.

The revised cooling rate in collision of $O(^3P)$ with thermal electrons with the $O(^1D)$ formation is given as

$$L(O(^1D)) = E_0 P_t . \tag{5}$$

The IZMIRAN model electron heating due to photo-electrons is provided by a solution of the Boltzmann equation for photoelectron flux (Pavlov, 1997). As the incident electrons penetrate the Earth's atmosphere they lose energy not only by ionizing and exciting the neutral constituents but also by heating thermal electrons, Q_{pr}. The updated IZMIRAN model uses the value of Q_{pr} given by Eq. (16) of Lummerzheim and Lilensten (1994).

The rate coefficient for quenching of $O^+(^2D)$ by atomic oxygen has not been measured in the laboratory and have assumed as $10^{-10} \, cm^3 \, s^{-1}$ (see discussion given by Pavlov 1997, 1998b). The MSIS-86 model (Hedin, 1987) with 3 h Ap indices is included in the IZMIRAN model to simulate magnetic storm effects on the neutral atmosphere. The IZMIRAN model uses the solar EUV fluxes from EUVAC model (Richards et al., 1994) in this work. At night our model includes ionization by scattered solar fluxes. The numerical technique for the numerical solution of the continuity, momentum and energy equations given by Marov and Kolesnichenko (1987) (Supplement II) is used in the IZMIRAN model. This numerical technique that we use is similar to that described by Hastings and Roble (1977). The solving patterns of the IZMIRAN model calculations were given by Marov and Kolesnichenko (1987), Pavlov (1989a, b, 1996, 1997, 1998b) and Pavlov and Buonsanto (1997).

3 Results

The 4–6 August, 1972 geomagnetic storm period occurred during medium solar activity (F10.7 = 146–147). The detailed description of the planetary magnetic index K_p and Dst for this period is given by Hoffman et al. (1975). A double sudden storm commencement occurred near the beginning of August 4 at 0119 UT and

0220 UT and was followed by a moderate main phase. During the main phase of the geomagnetic storm, the Dst index is decreased when the ring current builds up. The planetary index K_p reached 8_+ and 9_0 on 4 August at 0300 UT and 2100 UT. The recovery phase of the first geomagnetic storm began near 0700 UT on 4 August with $Dst = -118\gamma$. The next sudden commencement occurred at 2054 UT on 4 August.

Observations of the ion composition and electron temperature at 1400 km altitude and density height profiles from the altitude of the ISIS II spacecraft down to the F region, the intensity and the volume emission rate profile of the 630 nm oxygen emission in the SAR arc region are presented by Shepherd et al. (1975). The comparison between the ISIS II data and the IZMIRAN numerical results discussed here corresponds to the conditions of the SAR arc region in the Southern Hemisphere on 4 August, 1972 at 05:57:51 UT (the invariant latitude 60.7° and geographic longitude 170°, L shell value of the geomagnetic field is 4.175). The Explorer 45 (S^3-A) spacecraft observations at 0600 UT on 4 August placed the plasmapause at L = 4.2 (Hoffman et al., 1975) and this shows that the measured ISIS II SAR arc enhancements in T_e, and a part of the related SAR arc emission is closely associated with processes at the plasmapause.

To explain electron temperature enhancements and the associated SAR arcs the IZMIRAN model includes the additional heating rate, q, of the electron gas in plasmasphere due to Coulomb collisions between ring current ions and plasmaspheric electrons and ions and wave-particle interactions (Pavlov, 1997). There is no information available on the ring-current population and wave-particle interactions for this storm, and we are therefore forced to assume an additional heating rate, q, should be added to the normal photoelectron heating in the electron energy equation in the plasmasphere region $-s_0 < s < s_0$ above 5000 km along the magnetic field line in agreement with previous works of Pavlov (1996, 1997) concerning the rate of energy transfer from the energetic ring current ions to plasmaspheric electrons. We found that good agreement between the measured and modelled electron temperature is obtained if the value of $q = 1.05 \, eV \, cm^{-3} \, s^{-1}$ is selected during all storm time periods ($q = 0$ for undistributed conditions).

3.1 Electron flux spectra

The ISIS II soft particle spectrometer measured an energy spectrum of electrons and four of these spectra at pitch angles of $55°, 31°, 14°$, and $73°$ on 4 August, 1972 at 05:57:35 UT, 05:57:51 UT, 05:58:07 UT, and 05:58:23 UT are presented by Shepherd et al. (1975). The onset and the time duration of this soft electron flux event were not measured. The rarity of soft electron flux observations over SAR arcs does not allow us to evaluate the typical time characteristics of these events from other observations. Prasad et al. (1980) found that the soft electron flux data were obtained about 40 min before the occurrence of the SAR arc on orbit 8715 of

OGO 6 satellite and observed during orbit 8714 of OGO 6 satellite about 2 h 20 min before the birth of the SAR arc. Typical auroral events produced by electron precipitation are considered with a lifetime of electron precipitation events lasting from a few minutes to about an hour (Roble and Rees, 1977). As a result, we assume that the electron precipitation studied is realized from 05:30:00 UT to 6:30:00 UT, and the spectrum of incident electrons is the same during this time period.

We have no measurements of full pitch angular distributions of incident electrons for the studied SAR arc. As a result, we use the isotropy assumption for the incident electron flux. Our model calculates the fluxes of precipitating electrons integrated over pitch angles in the altitude range 120–1000 km covering the energy range from 0.5 eV to 52 keV if an incident electron flux, $F_\infty(E)$, is given at the upper boundary (see Appendix). The measured differential electron energy spectra, $U(E)$, shown in Fig. 4 of Shepherd *et al.* (1975) with energies from 6 eV to 8 eV at the mentioned four moments of time changed rapidly in a spatial sense. For energies below 6 eV and above 8 keV, where there are no measurements of $U(E)$, we assumed that $\log U(E) = A + B \log E$ (linear interpolation), and found the values of A and B from the measured spectra of Shepherd *et al.* (1975) at 6 eV and 8.5 eV (for $E < 6$ eV) and 5.2 keV and 8 keV (for $E > 8$ keV). We found that the best agreement between the modelled and measured volume emission rates at 630 nm is obtained if the approach of $F_\infty(E) = 0.2U(E)$ is used during the electron precipitation time period, where $U(E)$ is the value of the measured spectra at the pitch angle of 31° at 05:57:51 UT, E is an energy of electrons.

The dashed line in Fig. 1 shows the incident electron flux. The calculated flux of precipitating electrons at 300 km at 05:57:51 UT on August 4 is shown by solid line in Fig. 1. The incident flux can be seen centred at 21 eV in Fig. 1. At altitudes 1000 km and 300 km, there is very little degradation of this initial flux in the energy range between 50 eV and 250 eV but the degradation is very noticeable above 800–1000 eV. At 300 km, the electron flux is orders of magnitude larger than the incident electron flux at low energies 2–14 eV.

3.2 Modelling the SAR arc emission at 630 nm

Important characteristics of airglow are the volume emission rate and the integral intensity at 630 nm that are calculated by the model as

$$V_{630} = A_{630}[O(^1D)], \quad I_{630}(z) = \int_z^\infty V_{630}(h)dh, \quad (6)$$

where z is an altitude.

Figure 2 shows the measured (crosses) volume emission rates at 630 nm as extracted by Shepherd *et al.* (1980) from the tomographic inversion at 05:57:40–05:57:51 UT on August 4 in the SAR-arc region in comparison with the calculated (lines) 630 nm volume emission rates. The solid line shows the
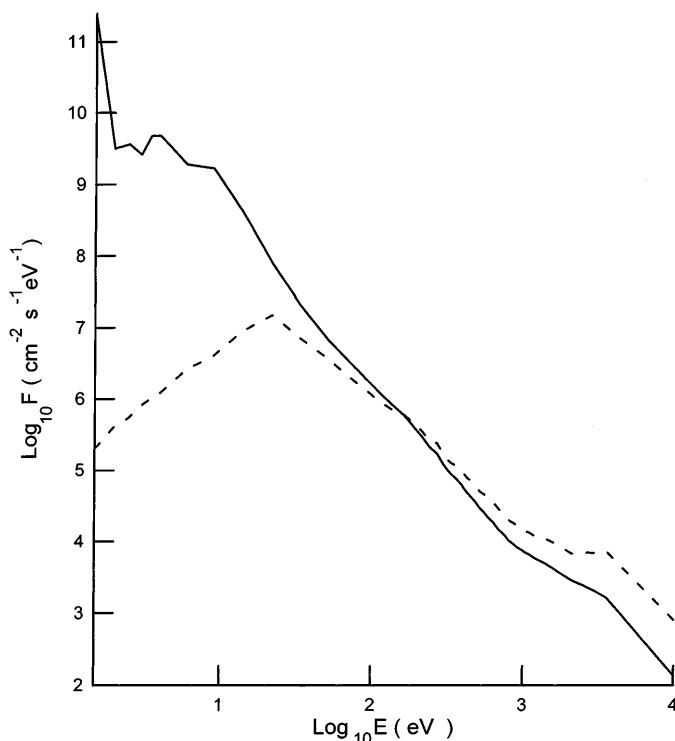
Fig. 1. The calculated flux of precipitating electrons at 300 km at 05:51:51 UT on August 4 in the SAR-arc region (*solid line*) for the incident electron flux (*dashed line*)
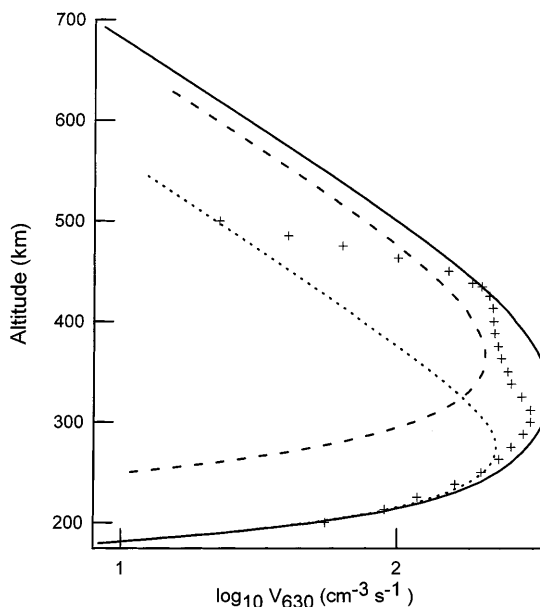
Fig. 2. Observed (*crosses*) and calculated (*lines*) 630 nm volume emission rates at 05:51:40–05:51:51 UT on August 4 in the SAR-arc region. The modelled volume emission rates were obtained when the IZMIRAN model includes the additional heating rate of the electron gas in the plasmasphere $q = 1.05\,\mathrm{eV\,cm^{-3}\,s^{-1}}$ and the fluxes of precipitating electrons of Fig. 1 (*solid line*) for the geomagnetic storm period. The *dotted line* shows the volume emission rate from the IZMIRAN model with the fluxes of precipitating electrons and without the additional heating rate of the electron gas in the plasmasphere. The *dashed line* represents the IZMIRAN model results with $q = 1.05\,\mathrm{eV\,cm^{-3}\,s^{-1}}$ in the plasmasphere and without $O(^1D)$ formation by collisions between $O(^3P)$ and precipitating electrons

IZMIRAN model results when the calculated fluxes of precipitating electrons of Fig. 1 and the additional heating rate of the electron gas in the plasmasphere of $1.05\,\mathrm{eV\,cm^{-3}\,s^{-1}}$ are used to agree the modelled and measured electron temperature as discussed later and to explain the excitation of the SAR arc observed. Our model calculates the 630 nm integral intensity above 350 km of 4.1 kR and the total 630 nm integral intensity, $I_{630}(0) = 8.1\,\mathrm{kR}$, which are slightly lower compared to $I_{630}(350) = 4.7\,\mathrm{kR}$ and $I_{630}(0) = 10.6\,\mathrm{kR}$ that were observed by Shepherd *et al.* (1980). This difference between the measured and modelled $I_{630}(z)$ and the big disagreement between the measured and calculated $V_{630}(z)$ at altitudes above 460–470 km is probably due to errors of the tomographic inversion method and errors of the IZMIRAN model calculations (effects of uncertainties in the solar fluxes and neutral temperature and densities on the calculated electron density and temperature, and effects of uncertainties in the fluxes of precipitating electrons on the $O(^1D)$ production rate). The heat flow requirement for the SAR arc was earlier estimated to be $0.16\,\mathrm{erg\,cm^{-2}\,s^{-1}}$ (Shepherd *et al.*, 1980) compared with the value $0.11\,\mathrm{erg\,cm^{-2}\,s^{-1}}$ of the flux of thermal electrons at 1400 km from IZMIRAN model.

The dotted line in Fig. 2 shows the volume emission rate from the IZMIRAN model with the fluxes of precipitating electrons and without the additional heating rate of the electron gas in the plasmasphere. The calculated integral intensity above 350 km and total integral intensity are about 1.1 kR and 3.8 kR, and these values are much smaller than those measured by Shepherd *et al.* (1980). This model gives the peak volume emission rate at 280 km in agreement with the measured one. However, the observed higher altitude component of $V_{630}(z)$, with its peak near 400 km cannot be explained by effects of precipitating electrons, and our results confirm the conclusion of Shepherd *et al.* (1980) that the upper component was excited through the $O(^1D)$ formation by collisions between $O(^3P)$ and thermal electrons.

The dashed line (Fig. 2) represents the IZMIRAN model results with $q = 1.05\,\mathrm{eV\,cm^{-3}\,s^{-1}}$ in the plasmasphere and without precipitation component to SAR arc generation by soft electrons. This model predicts $I_{630}(350) = 2.9\,\mathrm{kR}$ and $I_{630}(0) = 4.0\,\mathrm{kR}$ with the peak volume emission rate located at 360 km, which is lower than the measured higher altitude component peak of $V_{630}(z)$. Like the model result shown by the dotted line, the 630 nm integral intensity above 350 km and total 630 nm integral intensity given by this model are significantly smaller than those observed.

We conclude that the comparison between the measured and modelled $V_{630}(z)$, $I_{630}(350)$, and $I_{630}(0)$ indicates that our model reproduces major features of the data, and the 630 nm emission observed can be explained taking into account both the soft energy electron excited component with the incident electron flux given at 1000 km altitude as $0.2\,U(E)$ and the thermally excited component with $q = 1.05\,\mathrm{eV\,cm^{-3}\,s^{-1}}$ in the plasmasphere.

3.3 Modelling the SAR arc emission at 557.7 nm
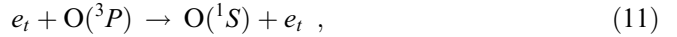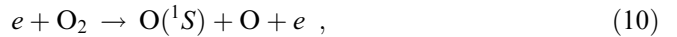
The 557.7 nm green line is the result of the transition

$$O(^1S) \rightarrow O(^1D) + h\nu \ , \tag{7}$$

with the Einstein coefficient $A_{557.7} = 1.22\,\mathrm{s^{-1}}$ given by Bhatia and Kastner (1995).

The volume emission rate and integral intensity at 557.7 nm are calculated by the model as

$$V_{557.7} = A_{557.7}[O(^1S)], \ I_{557.7}(z) = \int_z^\infty V_{557.7}(h)dh \tag{8}$$

Production processes for the $O(^1S)$ state considered in the present analysis include the direct excitation processes by precipitating (e) and thermal (e_t) electrons as

$$e + O(^3P) \rightarrow O(^1S) + e \ , \tag{9}$$

$$e + O_2 \rightarrow O(^1S) + O + e \ , \tag{10}$$

$$e_t + O(^3P) \rightarrow O(^1S) + e_t \ , \tag{11}$$

To calculate the production rate of $O(^1S)$ from the excitation of $O(^3P)$ by precipitating electrons we use the $O(^3P)$ excitation cross section given by Doering and Gulcicek (1989). The production rate of $O(^1S)$ following the dissociation of O_2 by precipitating electron impact is calculated by the use of the cross section for the production of $O(^1S)$ given by LeClair and McConkey (1993). The production rate of $O(^1S)$ due to process (11) can be calculated as by (Stubbe and Varnum, 1972)

$$P_{et}(O(^1S)) = N_e f_1 T_e[O] \ , \tag{12}$$

where $f_1(T_e) = \{8kT_e(\pi m_e)^{-1}\}^{0.5}\int_0^\infty \sigma_1(x)x\exp(-x)dx$, $x = E(kT_e)^{-1}$, and $\sigma_1(E)$ is the cross section for excitation of the $O(^1S)$ state by electrons.

The linear interpolation of $\sigma_1(E)$ measured by Doering and Gulcicek (1989) leads to the simple approach in calculations of $f_1(T_e)$ as

$$f_1(T_e) = 1.29 \cdot 10^{-11} T_e^{0.6}\exp(-E_{0S}/T_e) \ , \tag{13}$$

where $E_{0S} = 48618\,\mathrm{K}$ (or 4.1896 eV) is the energy of the $O(^1S)$ electron level given by Radzig and Smirnov (1980), and the unit of $f_1(T_e)$ is $\mathrm{cm^3\,s^{-1}}$.

We found that the value of maximum error for this analytical expression for $f_1(T_e)$ is less than 2% within the electron temperature range 1400–6000 K, and this accuracy is enough in our studies.

The chemical reactions

$$O_2^+ + e_t \rightarrow O(^3P) + O(^1S) \ , \tag{14}$$

$$N_2(A^3\Sigma_u^+, j) + O(^3P) \rightarrow N_2 + O(^1S) \ , \tag{15}$$
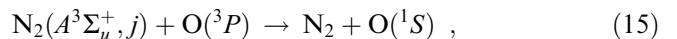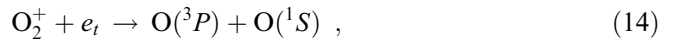
are also included in our study as production processes for the $O(^1S)$ state. The total rate coefficient of dissociative recombination of O_2^+ ions used in the IZMIRAN model is given by Pavlov (1997). The quantum yield of $O(^1S)$ from dissociative recombination of O_2^+ in the vibrational levels 1 and 2 may vary between

0.09 and 0.23 (Yee and Killeen, 1986), and we use a quantum yield of 0.15.

The interaction between $N_2(A^3\Sigma_u^+, j)$ at vibrational levels $j = 0$–7 with $O(^3P)$ give rise to many reaction channels with the total rate coefficients measured by Thomas and Kaufman (1985) for $j = 0, 1$ and De Benedicctis and Dilecce (1997) for $j = 2$–7. The formation products are enumerated: $N_2 + O(^1S)$, $N_2 + O(^3P)$, $N_2 + O(^1D)$, $NO + N(^4S)$, $NO + N(^2D)$. Piper (1981) has measured a value of 0.75 for the quantum yield of $O(^1S)$ from $N_2(A^3\Sigma_u^+, j = 0) + O(^3P)$. However, aurora and airglow emission studies (Gattinger *et al.*, 1985, Singh *et al.*, 1996) have suggested that this value is not appropriate for the other vibrational levels, and we use a value of 0.36 recommended by Singh *et al.* (1996).

Loss processes considered for the $O(^1S)$ state include radiative decay given by Eq. (7) and

$$O(^1S) \rightarrow O(^3P_1) + h\nu \; , \tag{16}$$

$$O(^1S) \rightarrow O(^3P_2) + h\nu \; , \tag{17}$$

with the Einstein coefficients $7.6 \cdot 10^{-2} \, \mathrm{s}^{-1}$ and $2.73 \cdot 10^{-4} \, \mathrm{s}^{-1}$ given by Bhatia and Kastner (1995), and the collisional deactivation processes

$$O(^1S) + O(^3P) \rightarrow O + O \; , \tag{18}$$

$$O(^1S) + O_2 \rightarrow O + O_2 \; . \tag{19}$$
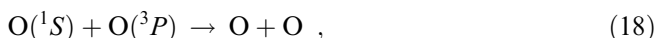
we use the rate coefficient of $5 \cdot 10^{-11} \exp(-305 \, T_n^{-1})$ $\mathrm{cm}^3 \, \mathrm{s}^{-1}$ for reaction (18) (Slanger and Black, 1981) and the rate coefficient of $4 \cdot 10^{-12} \exp(-865 \, T_n^{-1}) \, \mathrm{cm}^3 \, \mathrm{s}^{-1}$ for the reaction (19) (Slannger *et al.*, 1972).

The values of $V_{557.7}(z)$ and $I_{557.7}(z)$ are functions of $[N_2(A^3\Sigma_u^+, j)]$ which depends on number densities of $N_2(B^3\Pi_g^+, i)$ and $N_2(C^3\Pi_u, n)$ at vibrational levels "i" and "n" (Torr and Torr, 1982). To calculate the production rates, $Q(A, j)$, $Q(B, i)$, and $Q(C, n)$, of $N_2(A^3\Sigma_u^+, j)$, $N_2(B^3\Pi_g^+, i)$, and $N_2(C^3\Pi_u, n)$ from the excitation of the N_2 ground state by precipitating electrons we use the $N_2(A^3\Sigma_u^+)$, $N_2(B^3\Pi_g^+)$, and $N_2(C^3\Pi_u)$ excitation cross sections given by Majeed and Strickland (1997) and the Franc-Condon factors for these transitions presented by Gilmore *et al.* (1992) and Piper (1993).

The $N_2(C^3\Pi_u, n)$ loss processes include the radiative decay through the N_2 second positive bands as $N_2(C^3\Pi_u, n) \rightarrow N_2(B^3\Pi_g^+, i) + h\nu$. A complete set of the Einstein coefficients, $A_{\mathrm{ni}}(C, B)$, (Gilmore *et al.*, 1992) for these processes allows one to calculate

$$[N_2(C^3\Pi_u, n)] = Q(C, n) \left\{ \sum_i A_{\mathrm{ni}}(C, B) \right\}^{-1} . \tag{20}$$

Similarly, the N_2 first positive bands arise from the transitions $N_2(B^3\Pi_g^+, i) \rightarrow N_2(A^3\Sigma_u^+, j) + h\nu$, with the Einstein coefficients, $A_{ij}(B, A)$, given by Gilmore *et al.* (1992). This radiative decay determines the sinks of the $N_2(B^3\Pi_g^+, i)$ state, so that

$$[N_2(B^3\Pi_g^+, i)] = \left\{ Q(B, i) + \sum_n A_{\mathrm{ni}}(C, B)[N_2(C^3\Pi_u, n)] \right\}$$
$$\times \left\{ \sum_j A_{ij}(B, A) \right\}^{-1} \tag{21}$$

The model calculations include the collisional deactivation's processes for the $N_2(A^3\Sigma_u^+, j = 0$–7) state by $O(^3P)$, O_2, and NO with the measured rate coefficients, $K_j(O)$, $K_j(O_2)$, and $K_j(NO)$, given in Table II of De Benedicctis and Dilecce (1997). The reaction rate coefficient for quenching by N_2 is less than $10^{-18} \, \mathrm{cm}^3 \, \mathrm{s}^{-1}$ (Torr and Torr, 1982), and this process can be neglected in comparison with other quenchers of $N_2(A^3\Sigma_u^+, j)$. The $N_2(A^3\Sigma_u^+, j)$ loss processes considered include also radiative decay given by $N_2(A^3\Sigma_u^+, j) \rightarrow N_2(X^1\Sigma_g^+, v) + h\nu$ which determines the Vegard-Kaplan emission with the Einstein coefficients, $A_{jv}(A, X)$, given by Piper (1993). As a result, one obtains:

$$[N_2(A^3\Sigma_u^+, j)] = \left\{ Q(A, j) + \sum_i A_{ij}(B, A)[N_2(B^3\Pi_g^+, i)] \right\}$$
$$\times \left\{ \sum_v A_{jv}(A, X) + K_j(O) \right.$$
$$\left. + K_j(O_2) + K_j(NO) \right\}^{-1} . \tag{22}$$

As far as the authors know, the values of $K_j(O)$, $K_j(O_2)$, and $K_j(NO)$ are not measured and not calculated at vibrational levels $j > 7$, and our model calculates $[N_2(A^3\Sigma_u^+, j = 0, \dots 7)]$.

Shepherd *et al.* (1980) did not publish the measured $V_{557.7}(z)$, $I_{557.7}(z)$ in the studied SAR arc region, and we can only study the role of the sources of $O(^1S)$ described in production of the 557.7 nm green line in the altitude range from 120 km to 1000 km. Figure 3 shows the calculated altitude profile of the total volume emission rate at 557.7 nm (solid line) in the SAR arc region at 05:51:51 UT on 4 August, 1972, in comparison with the volume emission rate altitude profiles at 557.7 nm due to collisions of $O(^3P)$ with precipitating (dashed line 1) and thermal (dashed line 2) electrons, dissociative recombination of O_2^+ ions (dashed line 3), excitation of $O(^1S)$ in the reaction between $N_2(A^3\Sigma_u^+)$ and $O(^3P)$ (dashed line 4).

It is evident from the profiles shown in Fig. 3 that the excitation process producing $O(^1S)$ directly, electron impact on ambient $O(^3P)$, and the reaction of $N_2(A^3\Sigma_u^+)$ and $O(^3P)$ are the dominant production mechanisms for $O(^1S)$ below about 480 km. It is also apparent that the interaction between $N_2(A^3\Sigma_u^+, j)$ with $O(^3P)$ is the dominant production source of $O(^1S)$ at altitudes less than 190 km. We found also that the volume emission rate of $O(^1S)$ due to the production rate of $O(^1S)$ following the dissociation of O_2 by precipitating electrons is less than $0.2 \, \mathrm{cm}^{-3} \, \mathrm{s}^{-1}$, and this source of $O(^1S)$ production rate due to the three body recombination source $O + O + M$ can be considered as the source of $O(^1S)$ below 100–110 km (see, e.g., Singh *et al.*, 1997). Our model calculates $[O(^1S)]$ above 120 km, and this source of $O(^1S)$ is not included in the present analysis.
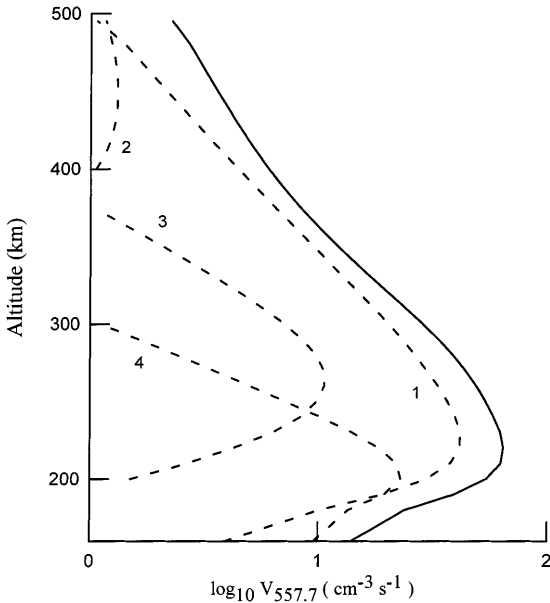
Fig. 3. The IZMIRAN model altitude profile of the total 557.7 nm volume emission rate (*solid line*) in comparison with the volume emission rate altitude profiles at 557.7 nm due to the sources of $O(^1S)$ (*dashed lines 1–5*) in the SAR arc region at 05:51:51 UT on 4 August, 1972. *Lines 1* and *2* represent the volume emission rates due to collisions of $O(^3P)$ with precipitating and thermal electrons, respectively. *Line 3* shows the volume emission rate determined by dissociative recombination of O_2^+ ions. The volume emission rate produced by excitation of $O(^1S)$ in the reaction between $N_2(A^3\Sigma_u^+)$ and $O(^3P)$ is shown by *curve 4*

The model predicts $I_{557.7}(350) = 101\,R$, $I_{557.7}(200) = 705\,R$, and $I_{557.7}(160) = 822\,R$ with the 557.7 nm peak volume emission rate located at 220 km, which is lower than the measured altitude component peaks of $V_{630}(z)$. One of the main properties of SAR arcs is that their dominant spectral line is the 630 nm line of atomic oxygen (Rees and Roble, 1975). Our results show that $I_{557.7}(z) << I_{630}(z)$, and the most likely identification of this feature is a SAR arc.

3.4 Effects of vibrational excited oxygen and nitrogen on electron density

The loss rate of $O^+(^4S)$ ions is given as

$$L = \sum_{v=0}^{\infty} [N_2(v)]K_{1v} + \sum_{v=0}^{\infty} [O_2(v)]K_{2v} \; , \tag{23}$$

where K_{1v} is the recombination rate coefficient of $O^+(^4S)$ ions with $N_2(v)$ (Schmeltekopf *et al.*, 1968; Hierl *et al.*, 1997; Pavlov, 1998b), K_{2v} is the recombination rate coefficient of $O^+(^4S)$ ions with $O_2(v)$ (Hierl *et al.*, 1997; Pavlov, 1998b), and v is the number of the N_2 or O_2 ground state vibrational level.

The IZMIRAN model calculates non-Boltzmann distributions of vibrationally excited molecular nitrogen and oxygen and includes the option to use the model of the Boltzmann distributions of $N_2(v)$ and $O_2(v)$ as (Pavlov, 1997, 1998b)

$$[N_2(v)]_B = [N_2(0)]_B \exp(-v\,3353\,T_v^{-1}) \; , \tag{24}$$

$$[O_2(v)]_B = [O_2(0)]_B \exp(-v\,2239\,T_{vib}^{-1}) \; , \tag{25}$$

where T_v is the vibrational temperature of $N_2(v)$, and T_{vib} is the vibrational temperature of $O_2(v)$.

The results of calculating $[O_2(v)]/[O_2(v)]_B$, T_{vib}, T_v, and T_n at hmF2 are presented in Fig. 4. The present study suggests that the deviations $[O_2(v)]$ from the Boltzmann distribution of Eq. (25) are not significant at vibrational levels $v < 3$, and the calculated distribution is highly non-Boltzmann at vibrational levels $v > 2$. For third, forth, and fifth vibrational levels of O_2 the ratios $[O_2(v)]/[O_2(v)]_B$ have their minimum values during the period 11.00–13.00 LT. The diurnal variations of the calculated $[O_2(v)]/[O_2(v)]_B$ are not significant at vibrational levels $v < 3$ and the value of this ratio is about 0.98–1.11 for $v = 1$ and 0.88–0.97 for $v = 2$. From the diurnal variations of the calculated vibrational (solid line) and neutral (dashed line) temperatures shown in Fig. 4 it follows that $T_{vib} < T_n$ and $T_v < T_n$ are realized in the atmosphere for the night-time periods where the
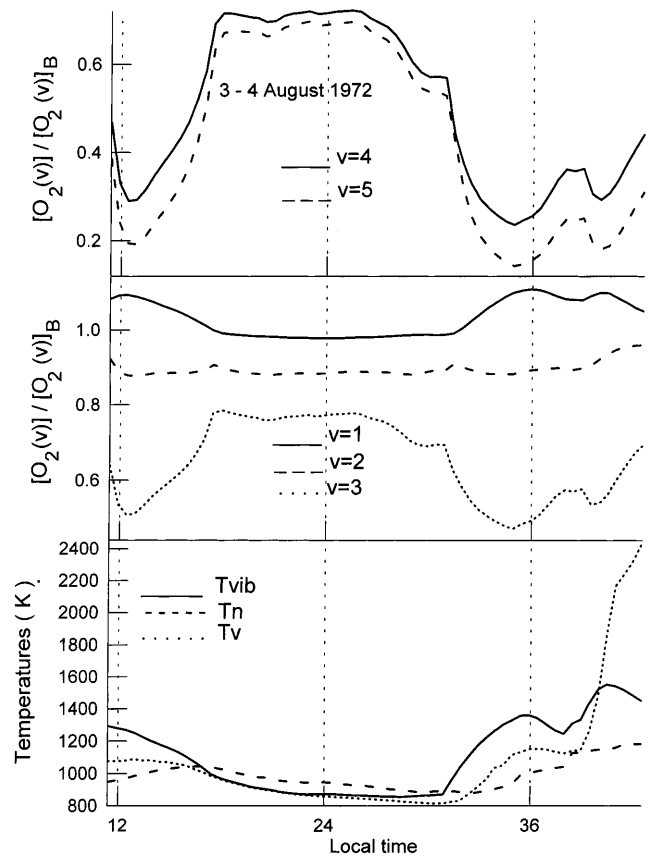
Fig. 4. The time variations of the vibrational temperatures of $[O_2]$ and $[N_2]$, the neutral temperature (*bottom panel*), and populations of the first five vibrational levels of O_2 ($v = 1, 2$, and 3 in the *middle panel* and $v = 4$ and 5 in the *top panel*) in comparison with the Boltzmann distribution of Eq. (25) during the 3–4 August period at the F2 peak altitude. The *solid lines* show the modelled T_{vib}, $[O_2(1)]/[O_2(1)]_B$, and $[O_2(4)]/[O_2(4)]_B$, the *dashed lines* show the modelled T_n, $[O_2(2)]/[O_2(2)]_B$, and $[O_2(5)]/[O_2(5)]_B$, and the *dotted lines* show the modelled T_v, and $[O_2(3)]/[O_2(3)]_B$

production frequencies of $O_2(v)$ and $N_2(v)$ are low. This means that for these periods the populations of $O_2(v)$ or $N_2(v)$ are less than the populations for a Boltzmann distribution with temperature T_n. During the daytime T_{vib} and T_v are larger than T_n due to the enhanced thermal excitation of O_2 and N_2 as a result of high thermal electron temperatures at F2-region altitudes. We found that $-77\,\text{K} \le T_{vib} - T_n \le 401\,\text{K}$ and $-88\,\text{K} \le T_v - T_n \le 1341\,\text{K}$. On 3–4 August the value of the vibrational temperature was not more than 1555 K for O_2 and 2539 K for N_2. In the SAR arc regions T_v and T_{vib} are larger than T_n due to the enhanced thermal excitation of N_2 and O_2 as a result of high thermal electron temperatures at F2- region altitudes after the beginning of the increase in T_e due to the additional heating rate of electrons.

The excitation of N_2 and O_2 by thermal electrons provides the main contribution to the values of $O_2(v)$ and $N_2(v)$ vibrational excitations (Pavlov and Namgaladze, 1988; Pavlov, 1989a, b, 1997, 1998b; Pavlov and Buonsanto, 1997). As a result, the values of $T_{vib} - T_n$ and $T_v - T_n$ increase with increasing the thermal electron production frequencies, $W(O_2)$ and $W(N_2)$, of the O_2 and N_2 vibrational quanta, correspondingly. Pavlov (1998a) found that the value of $W(N_2)$ increases with increasing T_e in the temperature range 300–6000 K. As seen from Fig. 4, due to this dependence, the value of T_v increases with increasing T_e in the SAR arc region. The value of $W(O_2)$ also increases with the increase of T_e (Pavlov, 1998c). However, unlike the dependence of $W(N_2)$ on T_e, this increase of $W(O_2)$ is very small in the temperature range 2500–4000 K as

$$W(O_2) \approx \text{const} \cdot N_e \ . \tag{26}$$

As seen from Eq. (26), the dependence of T_{vib} on T_e can be neglected in the SAR arc region, and this leads to $T_v > T_{vib}$. Equation (23) also explains the decrease of T_{vib} at night on 4 August as a result of day-night variations in N_e.

Figure 4 shows the diurnal variations of the modelled electron temperature at hmF2 (top panel), hmF2 (middle panel), and NmF2 (bottom panel) for the period 2–3 August, 1972. The top panel shows also the modelled electron temperature at 1400 km (dashed-dotted line) and the ISIS II spacecraft measurement of the electron temperature in the SAR arc region at 05:57:51 UT on 4 August, 1972, at 1400 km (cross). The solid lines show model results when vibrationally excited O_2 and N_2 are included in calculations of the $O^+(^4S)$ loss rate as given by Eq. (23). The dashed lines show model results when $N_2(v > 0)$ is not included and $O_2(v > 0)$ is included in calculations of the $O^+(^4S)$ loss rate:

$$L = K_{10}[N_2(v = 0)] + \sum_{v=0}^{\infty} K_{2v}[O_2(v)] \ . \tag{27}$$

The dotted lines in Fig. 5 are model results when the vibrationally excited nitrogen and oxygen are not included in the calculations of the loss rate the $O^+(^4S)$ ions:

$$L = K_{10}[N_2(v = 0)] + K_{20}[O_2(v = 0)] \ . \tag{28}$$
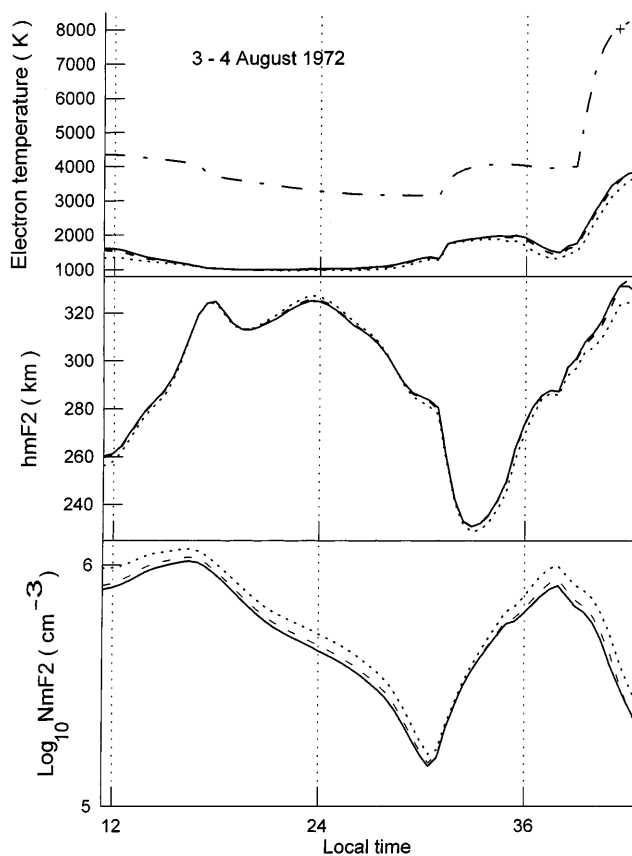
Fig. 5. The modelled NmF2 (*bottom panel*), hmF2 (*middle panel*), and electron temperatures at hmF2 and 1400 km (*top panel*) for the magnetically quiet and disturbed period 3–4 August, 1972. The modelled electron densities and temperatures were obtained with effects of $N_2(v)$ and $O_2(v)$ (*solid lines*) on the $O^+(^4S)$ loss rate, and when $N_2(v)$ was not included in the calculations (*dashed lines*) of this loss rate. The *dotted lines* give results without effects of $N_2(v)$ and $O_2(v)$ on the $O^+(^4S)$ loss rate. The *dashed-dotted line* represents the calculated electron temperature at 1400 km altitude. The ISIS II spacecraft measurement of the electron temperature in the SAR arc region at 05:51:51 UT on 4 August, 1972, at 1400 km is shown by a *cross*

From the comparison between solid and dashed lines of Fig. 5 it follows that the increase in the $O^+ + N_2$ loss rate due to vibrationally excited N_2 produces the 5–19% reductions in the calculated quiet daytime peak density and the 16–24% decrease in NmF2 in the SAR arc region. The comparison of dashed-dotted and dashed lines show that the increase in the $O^+ + N_2$ rate factor due to the vibrationally excited oxygen produces the 7–26% decrease in the calculated quiet daytime peak density and the 12–26% decrease in NmF2 in the SAR arc region. It should be noted that there is a large increase in the modelled NmF2 without vibrationally excited O_2 and N_2. The resulting effect on the NmF2 is a factor of 1.07–1.50 decrease in the quiet night-time and daytime peak densities and a factor of 1.30–1.56 in NmF2 in the SAR arc region using the IZMIRAN model when vibrationally excited O_2 and N_2 are not included in calculations of the $O^+(^4S)$ loss rate. The effect of vibrationally excited O_2 and N_2 on N_e is most pronounced during the daytime.

3.5 Electron density and temperature in the SAR arc region

For the studied geomagnetic storm period observations exist of the electron temperature and density height profiles from the altitude of the Isis II spacecraft down to the F region (Shepherd *et al.*, 1980). Figure 6 shows the measured (crosses) SAR arc electron densities (left panel) and temperatures (right panel) given by Shepherd *et al.* (1980) at 05:57:51 UT on August 4 in comparison with the modelled (lines) electron densities and temperatures. The model results were obtained with $N_2(v)$ and $O_2(v)$ (solid lines) and when the approaches of Eqs. (24) (dotted lines) and (25) (dashed lines) are used in the IZMIRAN model for the loss rate of the $O^+(^4S)$ ions. When vibrationally excited nitrogen and oxygen are included in the IZMIRAN model, the agreement between the measured N_e, T_e (crosses) and the modelled N_e, T_e (solid lines) is good. The measured N_e are higher than the modelled densities if $N_2(v)$ or $O_2(v)$ or $N_2(v)$ and $O_2(v)$ are not taken into account in calculations of the $O^+(^4S)$ loss rate. The effects of $N_2(v)$ and $O_2(v)$ on the calculation of T_e are negligible. The right panel of Fig. 6 also shows the calculated neutral temperature, and the vibrational temperatures of O_2 and N_2. It can been seen from a comparison of these temperatures that $T_v > T_{vib}$ above 240 km, and the neutral temperature is less than T_v or T_{vib}.
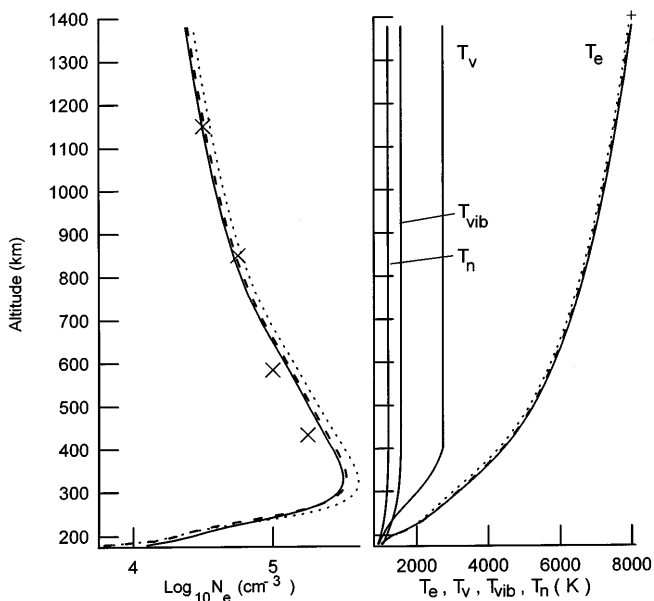
Fig. 6. Altitude profiles of the modelled (*lines*) electron densities (*left panel*) and temperatures (*right panel*) in the SAR arc region at 05:51:51 UT on 4 August, 1972, in comparison with the ISIS II spacecraft measurements (*crosses*) of the electron densities and temperatures. The modelled electron densities, N_e, and temperatures, T_e, were obtained with effects of $N_2(v)$ and $O_2(v)$ (*solid lines*) on the $O^+(^4S)$ loss rate, and when $N_2(v)$ was not included in the calculations (*dashed lines*) of this loss rate. The *dotted lines* give results without effects of $N_2(v)$, and $O_2(v)$ on the $O^+(^4S)$ loss rate. The *right panel* shows also the vibrational temperatures, T_{vib} and T_v, of O_2 and N_2, and the neutral temperature, T_n, from the IZMIRAN model in the SAR arc region at 05:51:51 UT on 4 August, 1972

We found that SAR arc thermal electron heating through energy loss of the precipitating electrons is most effective in the altitude range 180–230 km. The maximum increase of T_e due to the electron heating rate Q_{pr} is about 100 K at 200 km altitude. The energy where the fluxes of the precipitating electrons and thermal electrons cross over is less than 2 eV below 230 km altitude and larger than 2 eV above 230 km altitude in the region of high electron temperatures. The use of the IZMIRAN model without Q_{pr} leads to negligible decreases in the calculated electron temperature (40 K at 230 km altitude and 5 K at 300 km altitude) and total 630 nm integral intensity (16 R) in the SAR arc region in comparison with T_e and $I_{630}(0)$ calculated by using the rigorous approach with Q_{pr}.

3.6 Electron cooling rates

The relative magnitudes of the cooling rates are of particular interest for understanding the main processes which determine the electron temperature. The IZMIRAN model uses the generally accepted electron cooling rates due to electron-ion Coulomb collisions and elastic collisions of electrons with N_2, O_2, O, He, and H presented by Schunk and Nagy (1978), and the thermal electron impact excitation of $O_2(a^1\Delta_g)$ and $O_2(b^1\Sigma_g^+)$ given by Prasad and Furman (1973). The cooling rates of electrons which are in general use (see Schunk and Nagy, 1978) are the thermal electron impact excitation of the fine structure levels of the ground state of atomic oxygen of Hoegy (1976), the electron cooling rates given by Stubbe and Varnum (1972) and Prasad and Furman (1973) for vibrational excitation of N_2 and O_2, the rate of electron cooling through rotational excitation of N_2 and O_2 presented by Stubbe and Varnum (1972) and Dalgarno *et al.* (1968), and the electron energy loss arising from electron-impact-induced transitions $^3P \rightarrow {}^1D$ for atomic oxygen of Stubbe and Varnum (1972).

Pavlov (1998a, c) calculated and fit to the new analytical expressions the electron cooling rates by rotational and vibrational excitation of N_2 and O_2 using the revised quadrupole moments of O_2 and N_2 averaged over the ground vibrational state of O_2 and N_2, and the revised vibrationally excited O_2 and N_2 cross sections, and these new electron cooling rates were used in the IZMIRAN model of Pavlov (1998b). Pavlov and Berrington (1999) used the theoretical $O(^3P)$ excitation cross sections of Bell *et al.* (1998) to calculate and to fit to a new analytical expression for atomic oxygen fine structure cooling rate of thermal electrons, and this new approach is included in the updated IZMIRAN model. At the F region altitudes of the ionosphere, this new cooling rate is less than the currently accepted fine structure cooling rate of Hoegy (1976) by a factor of 2–4, and this cooling is not the dominant electron cooling process in the F region of the ionosphere at middle latitudes (Pavlov and Berrington, 1999). The revised IZMIRAN model cooling due to electronic excitation of $O(^1D)$ is given by Eq. (5).

The solid lines in Fig. 6 show a comparison of the IZMIRAN model electron cooling rates with the currently accepted cooling rates (dashed lines) in the studied SAR arc region at 05:51:51 UT on 4 August 1972. The energy exchange between the electron and ion gases (curve 1), the revised electron cooling rates due to excitation of O to the ^1D state (curve 4), and by vibrational excitation of N_2 (curve 2) and O_2 (curve 3) are the dominant cooling channels above 200 km. The IZMIRAN model fine structure cooling by O (curve 5) and the electron cooling rate by rotational excitation of N_2 (curve 6) are much less than the mentioned cooling rates in the SAR arc region. We found that the contribution of the cooling of electrons by low-lying electronic excitation of $O_2(a^1\Delta_g)$ and $O_2(b^1\Sigma_g^+)$ (curve 8), and the revised cooling by rotational excitation of O_2 (curve 7) can be neglected above 200 km altitude as they are not more than 1% of the total cooling rate during the quiet and geomagnetic storm period 3–4 August, 1972. The cooling of electrons due to total elastic electron-neutral collisions (curve 9) varies between 1% to 5% of the total cooling rate in the altitude range 200–700 km and can be considered small in the ionosphere in comparison with the total cooling rate (curve 10).

The dashed lines of Fig. 7 show the calculated cooling rates $L(O(^3P_j))$, $L(O(^1D))$, $L(N_2(v))$, $L(O_2(v))$, $L(N_2(rot))$, and $L(O_2(rot))$ of electrons due to the excitation of fine structure levels in O, electron-impact-induced transitions $^3P \rightarrow {}^1D$ for atomic oxygen, vibrational excitation of N_2 and O_2, and rotational excitation of N_2 and O_2 which are currently used in models of the ionosphere (Schunk and Nagy, 1978). It is clear from Fig. 7 that the IZMIRAN model value of $L(O(^1D))$ (solid line 4) is lower than those of Stubbe and Varnum (1972) (dashed line 4) by a factor of 1.2–2.6 in the height range 260–600 km. The ratio of the IZMIRAN model $L(O_2(v))$ (solid line 3) to $L(O_2(v))$ given by Prasad and Furman

(1973) (dashed line 3) is about 2–7 in the region between 200 and 500 km in altitude. The IZMIRAN model $L(N_2(v))$ (solid line 2) is higher than those of Stubbe and Varnum (1972) (dashed line 2) by a factor of 3–6 below 220 km and only up to a factor of 1.4 in the altitude range 230–500 km. The ratio of the generally accepted $L(O(^3P_j))$ given by Hoegy (1976) (dashed line 5) to $L(O(^3P_j))$ given by Pavlov and Berrington (1999) (solid line 5) is about 2–6 in the region between 200 and 700 km in altitude.

It was shown that the rate of electron energy loss associated with rotational transitions in N_2 of Stubbe and Varnum (1972) must be multiplied by a factor of 1.255 (Pavlov, 1998a), and the rate of electron energy loss associated with rotational transitions in O_2 given by Dalgarno *et al.* (1968) must be decreased by a factor of 13 (Pavlov, 1998c). These ratios determine the difference between the IZMIRAN model electron cooling rates due to rotational excitation of N_2 (solid line 6 of Fig. 7) and O_2 (solid line 7 of Fig. 7) and those of Stubbe and Varnum (1972) (dashed line 6 of Fig. 7) and Dalgarno *et al.* (1968) (dashed line 7 of Fig. 7) which are in general use.

The electron temperature is determined from the electron energy balance by competition between total heating, cooling, and energy flow processes. To calculate the total cooling rate of thermal electrons, it is necessary to sum up all energy loss rates mentioned for electrons. The ratio of the resulting IZMIRAN model total cooling rate (solid line 10 of Fig. 7) to the generally accepted total cooling rate of Schunk and Nagy (1978) (dashed line 10 of Fig. 7) is about 0.8–1.4 in the SAR arc region between 200 and 700 km in altitude.

4 Conclusions

The comparison of the measurements of the electron density and temperature, the integral airglow intensity
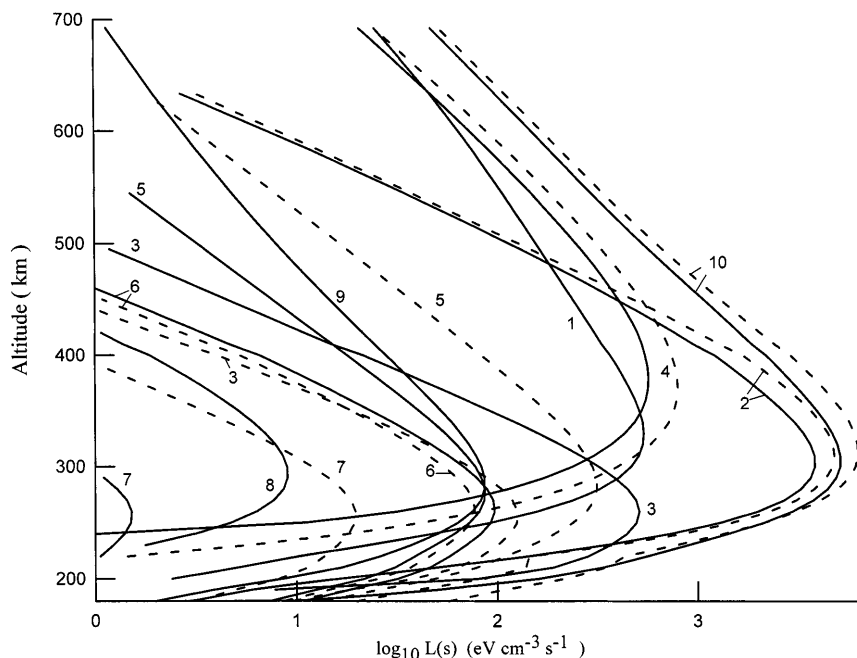
Fig. 7. The IZMIRAN model (*solid lines*) and generally accepted (*dashed lines*) altitude profiles of electron cooling rates, L(s), in the SAR arc region at 05:51:51 UT on 4 August, 1972. *Line 1* gives the cooling due to Coulomb collisions electrons with ions. The cooling rates by vibrational excitation of N_2 and O_2 are shown by *curves 2* and *3*. *Lines 4* represent the electron cooling rate in collision of $O(^3P)$ with thermal electrons with the $O(^1D)$ formation. *Lines 5* show the electron cooling rates due to collisions of electrons with atomic oxygen which excite fine structure transitions among the ground state levels of atomic oxygen. The cooling rates by rotational excitation of N_2 and O_2 are shown by *curves 6* and *7*. *Line 8* gives the cooling due to the thermal electron impact excitation of $O_2(a^1\Delta_g)$ and $O_2(b^1\Sigma_g^+)$, and the total elastic cooling rate by elastic collisions of electrons with N_2, O_2, O, He, and H is shown by *curve 9*. *Lines 10* represent the total cooling rates of electrons

and volume emission rate at 630 nm in the SAR arc region, which were obtained on the Isis II spacecraft on 4 August 1972, with the model results is presented. The model used is an enhanced version of the IZMIRAN model we have steadily developed over the years. The major enhancement to the IZMIRAN model developed in this study is the use of the analytical yield spectrum approach developed by Green *et al.* (1977), Jackman and Green (1979), Singhal *et al.* (1979), Singhal and Green (1981), and Haider and Singhal (1983) to calculate the fluxes of precipitating electrons in the altitude range 120–1000 km in the Northern and Southern Hemispheres if an incident electron flux is given at the upper boundary. Using this approach the IZMIRAN model calculates the additional production rates of N_2^+, O_2^+, $O^+(^4S)$, $O^+(^2D)$, $O^+(^2P)$, and $O^+(^2P)$ ions, $O(^1D)$, $N_2(C^3\Pi_u, n)$, $N_2(B^3\Pi_g^+, i)$, $N_2(A^3\Sigma_u^+, j)$, and $O(^1S)$, and the additional thermal electron heating in the SAR arc regions in the Northern and Southern Hemispheres due to fluxes of precipitating electrons. In order to bring the measured and modelled electron temperatures into agreement, the additional heating electron rate of 1.05 eV cm^{-3} s^{-1} providing the heat flux to the SAR-arc region was added to the energy balance equation of electrons at the altitude above 5000 km during the main phase of the geomagnetic storm.

We found that the best agreement between the modelled and measured volume emission rates at 630 nm is obtained if the approach of $F_\infty(E) = 0.2\,U(E)$ for the incident electron flux at 1000-km altitude is used during all storm time period where $U(E)$ is the value of the measured spectra at the pitch angle of 31° at 05:57:51 UT. The IZMIRAN model calculates the 630 nm integral intensity above 350 km of 4.1 kR and the total 630 nm integral intensity of 8.1 kR, which are slightly lower compared to 4.7 kR and 10.6 kR that were observed by Shepherd *et al.* (1980). We conclude that the comparison between the measured and modelled 630 nm emissions indicates that our model reproduces major features of the data. The 630 nm emission observed can be explained taking into account both the soft energy electron excited component and the thermally excited component.

The deviations from the Boltzmann distribution for the first five vibrational levels of O_2 were calculated. The present study suggests that the deviations from the Boltzmann distribution are not significant. The calculations also showed that the O_2 and N_2 vibrational temperatures during the quiet periods are less than during the magnetic storm periods. During the daytime the high vibrational temperatures stem from the enhanced thermal excitation of O_2 and N_2 as a result of high thermal electron temperatures at F2-region altitudes, while the decrease in the vibrational temperatures compared to the regular temperature is due to the decreases in the electron density and the neutral temperature.

We found that the inclusion of $N_2(v > 0)$ and $O_2(v > 0)$ in the calculations of the $O^+(^4S)$ loss rate improves the agreement between the calculated N_e and the data on 4 August, 1972 and the $N_2(v > 0)$ and $O_2(v > 0)$ effects are enough to explain the electron density depression in the SAR arc F-region and above F2 peak altitude. Our calculations show that the increase in the $O^+ + N_2$ rate factor due to the vibrationally excited nitrogen produces the 5–19% reductions in the calculated quiet daytime peak density and the 16–24% decrease in NmF2 in the SAR arc region. The increase in the $O^+ + N_2$ loss rate due to vibrationally excited O_2 produces the 7–26% decrease in the calculated quiet daytime peak density and the 12–26% decrease in NmF2 in the SAR arc region. The effect of vibrationally excited O_2 and N_2 on N_e is most pronounced during the daytime.

The electron energy balance has been studied by employing the revised energy loss rates. We evaluated the role of the electron cooling rates by low-lying electronic excitation of $O_2(a^1\Delta_g)$ and $O_2(b^1\Sigma_g^+)$, and rotational excitation of O_2, and found that the effect of these cooling rates on T_e can be considered negligible above 200 km altitude during the quiet and geomagnetic storm period 3–4 August, 1972. The energy exchange between electron and ion gases, the cooling rate in collisions of $O(^3P)$ with thermal electrons with excitation of $O(^1D)$, and the electron cooling rates by vibrational excitation of N_2 and O_2 and are the largest cooling rates above 200 km in the SAR arc region on 4 August, 1972.

The enhanced IZMIRAN model used for this study calculates number densities of $N_2(B^3\Pi_g^+, i)$, $N_2(C^3\Pi_u, n)$, $N_2(A^3\Sigma_u^+, j)$, and $O(^1S)$, and the volume emission rate and integral intensity at 557.7 nm in the region between 120 and 1000 km in altitude in the SAR arc region on 4 August, 1972. We found that the excitation process producing $O(^1S)$ directly, electron impact on ambient $O(^3P)$, and the reaction of $N_2(A^3\Sigma_u^+)$ and $O(^3P)$ are the dominant production mechanisms for $O(^1S)$ below about 480 km, and the interaction between $N_2(A^3\Sigma_u^+, j)$ and $O(^3P)$ is the dominant production source of $O(^1S)$ at altitudes less than 190 km. We found also that the production rate of $O(^1S)$ following the dissociation of O_2 by precipitating electrons can be neglected in comparison with other sources of $O(^1S)$. One of the main properties of SAR arcs is that their dominant spectral line is the 630 nm line of atomic oxygen. Our results shown that $I_{557.7}(z) << I_{630}(z)$ in agreement with a classical SAR-arc property.

Appendix

Model of precipitating electron fluxes
To calculate an equilibrium electron flux in the Earth's atmosphere we use the analytical spatial yield approach developed by Haider and Singhal (1983). Although they considered the spatial yield spectra for electron energy degradation in the non-homogeneous

atmosphere, some formulas in their paper are valid only in the case of homogeneous gas mixtures. Because the generalization of this relationships maybe not so evident, as well as for consistency within the present work, we reproduce here some formulas for calculations of electron fluxes, where the non-homogeneity of the atmosphere is taken into account in the explicit form.

Assuming that velocities of electrons are directed along the magnetic field line and an incident electron flux, $F_\infty(E)$, is given as an upper boundary condition, the flux of precipitating electrons is calculated by Haider and Singhal (1983) in the energy range 2 eV−10 keV as

$$F(E,s) = \frac{\rho(s)}{\sum_k n_k(s)\sigma_k(E)} \int_{E_{\min}}^{E_{\max}} U^c(E,z(s,E_0),E_0)F_\infty(E_0)dE_0 \; , \tag{A1}$$

where s is the distance along the magnetic field line from the upper boundary expressed in cm, ρ is the mass density of the atmosphere expressed in gm cm^{-3}, n_k denotes the number density of the k-th neutral component of the atmosphere, the unit of n_k is cm^{-3}, E_{min} and E_{max} are the boundaries of the energy range for incident electrons in eV, σ_k is the total inelastic cross section of the k-th neutral component of the atmosphere expressed in cm^{-2}, z is an "effective" distance (gm cm^{-2}), and U^c is a composite three-dimensional yield spectrum (eV^{-1} gm^{-1} cm^2), the units of F and F_∞ are cm^{-2} s^{-1} eV^{-1}.

An "effective" distance, z, depends on the energy of incident electrons and is calculated as

$$z(s,E_0) = \int_0^s ds' \rho(s')/\bar{R}(E_0,s') \; . \tag{A2}$$

An effective scaling factor $\bar{R}$ in Eq. (A2) is given by

$$\bar{R}(E_0,s) = \frac{\sum_k n_k(s)Z'_k(E_0)R_k(E_0)}{\sum_k n_k(s)Z'_k(E_0)} \; , \tag{A3}$$

where R_k is a scaling factor for k-th neutral component.

It should be noted that a scaling factor $\bar{R}$ depends only on ratios of Z'_k/Z'_1. As a result, it is possible to assume that $Z'_1(E_0) = 1$ for some neutral component (N$_2$ in our calculations) and calculate $Z'_k(E_0)$ for other neutral components as

$$Z'_k(E_0) = \frac{Z'_1(E_0)}{E_0-E_m} \int_{E_m}^{E_0} \frac{\sigma_{Tk}(E)}{\sigma_{T1}(E)} dE \; , \tag{A4}$$

where σ_{Tk} is the total (elastic + inelastic) cross section of gas "k", E_m is the minimum threshold energy for the states considered (in our calculations we assume $E_m \approx 0$ eV).

Singhal *et al.* (1980) and Singhal and Green (1981) give analytical formulas to calculate values of R_k for molecular nitrogen and atomic oxygen (see also the paper by Haider and Singhal, 1983, for correct values of constants for atomic oxygen). A scale factor for molecular oxygen can be found from the relationship of Haider and Singhal (1983) as

$$\frac{R_{O_2}(E_0)}{R_{N_2}(E_0)} = \frac{m_{O_2}}{m_{N_2}}\frac{Z_{N_2}(E_0)}{Z_{O_2}(E_0)} \; . \tag{A5}$$

Composite yield function is defined in terms of "partial" yield functions, U_k, for each component of gas mixture as

$$U^c(E,z,E_0) = \frac{\sum_k n_k(s)Z_k(E_0)U_k(E_0,z(E_0,s))}{\sum_k n_k(s)Z_k(E_0)} \; . \tag{A6}$$

It should be noted that composite yield function depends only on ratios of Z_k/Z_1. As a result, it is possible to assume that $Z_1(E_0) = 1$ for some neutral component (N$_2$ in our calculations) and calculate $Z_k(E_0)$ for other neutral components as

$$Z_k(E_0) = \frac{Z_1(E_0)}{E_0-E_m} \int_{E_m}^{E_0} \frac{\sigma_k(E)}{\sigma_1(E)} dE \; , \tag{A7}$$

where σ_k and σ_1 are inelastic cross sections for k-th and 1st components.

Analytical formulas for partial yield functions in Eq. (A6) for molecular nitrogen and atomic oxygen are given by Singhal *et al.* (1980) and Singhal and Green (1981). In constructing a partial yield function for molecular oxygen we use the parameters for partial molecular nitrogen yield function as suggested by Haider and Singhal (1983).

For O, the elastic cross section employed in the electron transport code was drawn from the work of Williams and Allen (1989) for energies below 8.7 eV, and, above 8.7 eV, we have adopted the elastic cross section of Joshipura and Patel (1993) up to 1 keV. The integral cross section of Doering and Gulcicek (1989) for electron collisional excitation of the $^3P \rightarrow {}^1D$ transition in atomic oxygen is a part of the total inelastic cross section for O presented by Laher and Gilmore (1990). We use the total inelastic cross section of Laher and Gilmore (1990) which is changed by taking into account the revised cross section for the $^3P \rightarrow {}^1D$ transition measured by Doering (1992).

For O$_2$, the total elastic and inelastic cross sections are taken from Kanic *et al.* (1993) below 1 keV. The N$_2$ elastic cross section of Iticawa (1994) for electron energies below 1 keV is used in our model. The N$_2$ total inelastic cross section is given by Majed and Strickland (1997) below 1 keV and we employ this cross section with some modification. The N$_2$ vibrational excitation cross sections used by Majed and Strickland (1997) in calculations of the N$_2$ total inelastic cross section were replaced by the N$_2$ vibrational excitation cross sections of Robertson *et al.* (1997) for vibrational levels $v = 1$ and 2, and those of Schulz (1976) for $v = 3$–10 with the normalization factor of 0.7 given by Haddad (1984) (see details in Pavlov, 1998a).

Note that for electron impact energy $E > 1000$ eV we approximate the total elastic and inelastic cross sections with the formulas of Born-Bethe theory given by Laher and Gilmore (1990) for O and Liu (1987) for N$_2$ and O$_2$.

References

Albritton, D. L., I. Dotan, W. Lindinger, W. McFarland, J. Telling-huisen, and F. C. Fehsenfeld, Effects of ion speed distributions in flow-drift tube studies of ion-neutral reactions, *J. Chem. Phys.* **66,** 410–421, 1977.

Banks, P. M., C. R. Chappel, and A. F. Nagy, A new model for the interaction of auroral electrons with the atmosphere: spectral degradation, backscatter, optical emission, and ionization, *J. Geophys. Res.,* **79,** 1459–1470, 1974.

Bell, K. L., K. A. Berrington, and M. R. J. Thomas, Electron impact excitation of the ground-state ^{3}P fine-structure levels in atomic oxygen, *Mon. Not. R. Astron. Soc.* **293,** L83–L87, 1998.

Bhatia, A. K., and S. O. Kastner, The neutral oxygen spectrum. I. Collisionally excited level populations and line intensities under optically thin conditions, *Astrophys. J. Suppl. Ser.,* **96,** 325–341, 1995.

Dalgarno, A., M. B. McElroy, and J. C. G. Walker, The effect of oxygen cooling on ionospheric electron temperatures, *Planet. Space Sci.,* **16,** 1371–1380, 1968.

De Benedicctis, S., and G. Dilecce, Rate constants for deactivation of N$_2$(A)v = 2–7, *J. Chem. Phys.,* **107,** 6219–6229, 1997.

Doering, J. P., Absolute differential and integral electron excitation cross-sections for atomic oxygen. 9. Improved cross sections for the ^{3}P $\rightarrow {}^1$D transition from 4.0 to 30 eV, *J. Geophys. Res.,* **97,** 19 531–19 534, 1992.

Doering, J. P., and E. E. Gulcicek, Absolute differential and integral electron excitation cross- sections for atomic oxygen. 7. The ^{3}P $\rightarrow {}^1$D and ^{3}P $\rightarrow {}^1$S transitions from 4.0 to 30 eV, *J. Geophys. Res.,* **94,** 1541–1546, 1989.

Foster, J. C., M. J. Buonsanto, M. Mendillo, D. Nottingham, F. J. Rich, and W. Denig, Coordinated stable auroral red arc observations: relationship to plasma convection, *J. Geophys. Res.,* **99,** 11 429–11 439, 1994.

Gattinger, R. L., F. R. Harris, and A. Vallance Jones, The height, spectrum and mechanism of type-B red aurora and its bearing on the excitation of O(^{1}S) in aurora, *Planet. Space Sci.*, **33**, 207–215, 1985.

Gilmore, F. G., R. R. Laher, and P. J. Espy, Frank-Condon factors, r-centroids, electronic transition moments, and Einstein coefficients for many nitrogen and oxygen band systems, *J. Phys. Chem. Ref. Data*, **21**, 1005–1107, 1992.

Green, A. E. S., C. H. Jackman, and R. H. Garvey, Electron impact on atmospheric gases. 2. Yield spectra, *J. Geophys. Res.*, **82**, 5104–5111, 1977.

Gurgiolo, C., D. W. Slater, J. D. Winningham, and J. L. Burch, Observation of a heated electron population associated with the 6300 A SAR arc emission, *Geophys. Res. Lett.*, **9**, 965–968, 1982.

Haddad, G. N., Cross sections for electron scattering in nitrogen, *Austr. J. Phys.*, **37**, 484–494, 1984.

Haider, S. A., and R. P. Singhal, Analytical yield spectrum approach to electron energy degradation in Earth's atmosphere, *J. Geophys. Res.*, **88**, 7185–7189, 1983.

Hasting, J. T., and R. G. Roble, An automatic technique for solving coupled vector systems of non-linear parabolic partial differential equations in one space dimension, *Planet. Space. Sci.*, **25**, 209–215, 1977.

Hierl, M. P., I. Dotan, J. V. Seeley, J. M. Van Doren, R. A. Morris, and A. A. Viggiano, Rate constants for the reactions of O$^+$ with N$_2$ and O$_2$ as a function of temperature (300–1800 K), *J. Chem. Phys.*, **106**, 3540–3544, 1997.

Hedin, A. E., MSIS-86 thermospheric model, *J. Geophys. Res.*, **92**, 4649–4662, 1987.

Hoegy, W. R., New fine structure cooling rate, *Geophys. Res. Lett.*, **3**, 541–544, 1976.

Hoffman, R. A., L. J. Cahll, Jr., R. R. Anderson, N. C. Maynard, P. H. Smith, T. A. Fritz, D. J. Williams, A. Konradi, and D. A. Gurnett, Explorer 45 (S^3-A) observations of the magnetosphere and magnetopause during the August 4–6, 1972, magnetic storm period, *J. Geophys. Res.*, **80**, 4287–4296, 1975.

Hwang, W., Y. -K. Kim, and M. E. Rudd, New model for electron-impact ionization cross sections of molecules, *J. Chem. Phys.*, **104**, 2956–2966, 1996.

Itikawa, Y., Electron collisions with N$_2$, O$_2$, and O: what we do and not know, in *Advances in Atomic, Molecular and Optical Physics*, **33**, Academic Press, New York, 253–273, 1994.

Jackman, C. H., and A. E. S. Green, Electron impact on atmospheric gases. 3. Spatial yield spectra for N$_2$, *J. Geophys. Res.*, **84**, 2715– 2724, 1979.

Joshipura, K. N., and P. M. Patel, Cross sections of e$^-$-O scattering at intermediate and high energies (E$_i$ = 8.7–1000 eV), *Phys. Rev.*, **48**, 2464–2467, 1993.

Kanic, I., S. Trajmar, and J. C. Nickel, Total electron scattering and electronic state excitations cross sections for O$_2$, CO$_2$, and CH$_4$, *J. Geophys. Res.*, **98 E**, 7447–7460, 1992.

Kozyra, J. U., A. F. Nagy, and D. W. Slater, High-altitude energy source(s) for stable auroral red arcs, *Rev. Geophys.*, **35**, 155–190, 1997.

Laher, R. R., and F. R. Gilmore, Updated excitation and ionization cross sections for electron impact on atomic oxygen, *J. Phys. Chem. Ref. Data*, **19**, 277–305, 1990.

LaValle, S. R., and D. D. Elliott, Observations of SAR arcs from OV1-10, *J. Geophys. Res.*, **77**, 1802–1809, 1972.

LeClair, L. R., and J. W. McConkey, Selective detection of O(^{1}S$_0$) following electron impact dissociation of O$_2$ and N$_2$O using a XeO* conversion technique, *J. Chem. Phys.*, **99**, 4566–4577, 1993.

Liu, J. W., Total cross sections for high-energy electron scattering by H$_2$($^1\Sigma_g^+$), N$_2$($^1\Sigma_g^+$), and O$_2$($^3\Sigma_g^-$), *Phys. Rev. A*, **35**, 591–597, 1987.

Lummerzheim, D., and J. Lilensten, Electron transport and energy degradation in the ionosphere: evaluation of the numerical solution, comparison with laboratory experiments and auroral observations, *Ann. Geophysicae*, **12**, 1039–1051, 1994.

Majeed, T., and D. J. Strickland, New survey of electron impact cross sections for photoelectron and auroral electron energy loss calculations, *J. Phys. Chem. Ref. Data*, **26**, 335–349, 1997.

Maier, E. J., S. Chandra, L. Brace, L. et al. The SAR arc event observed during the December 1971 magnetic storm, *J. Geophys. Res.*, **80**, 4591–4597, 1975.

Mantas, G. P., and C. G. Walker, The penetration of soft electrons into the ionosphere, *Planet. Space Sci.*, **24**, 409–423, 1976.

Marov, M. J., and A. V. Kolesnichenko, *Introduction into aeronomy of planets*, (in Russian), Nauka, Moscow, 1987.

McFarland, M., D. L. Albritton, F. C. Fehsenfeld, E. E. Ferguson, and A. L. Schmeltekopf, Flow-drift technique for ion mobility and ion-molecule reaction rate constant measurements, II. Positive ion reaction of N$^+$, O$^+$, and N$_2^+$ with O$_2$ and O$^+$ with N$_2$ from thermal to 2 eV, *J. Chem. Phys.*, **59**, 6620– 6628, 1973.

Newton, G. P., and J. C. G. Walker, Electron density decrease in SAR arcs resulting from vibrationally excited nitrogen, *J. Geophys. Res.*, **80**, 1325–1327, 1975.

Newton, G. P., J. C. G. Walker, and P. H. E. Meijer, Vibrationally excited nitrogen in stable auroral red arcs and its effect on ionospheric recombination, *J. Geophys. Res.*, **79**, 3807–3818, 1974.

Pavlov, A. V., On the O$_2^*$ content in the upper atmosphere and the effect of N$_2^*$ and O$_2^*$ on the electron density (in Russian), *Geomagn. Aeron.*, **29**, 818–823, 1989a.

Pavlov, A. V., About the role of vibrationally excited nitrogen in the sabauroral red arc region (in Russian), *Geomagn. Aeron.*, **29**, 948–953, 1989b.

Pavlov, A. V., Mechanisms of the electron density depletion in the SAR arc region, *Ann. Geophysicae*, **14**, 211–221, 1996.

Pavlov, A. V., Subauroral red arcs as a conjugate phenomenon: comparison of OV1-10 satellite data with numerical calculations, *Ann. Geophysicae*, **15**, 984–998, 1997.

Pavlov, A. V., New electron energy transfer rates for vibrational excitation of N$_2$, *Ann. Geophysicae*, **16**, 176–182, 1998a.

Pavlov, A. V., The role of vibrationally excited oxygen and nitrogen in the ionosphere during the undisturbed and geomagnetic storm period of 6–12 April 1990, *Ann. Geophysicae*, **16**, 589–601, 1998b.

Pavlov, A. V., New electron energy transfer and cooling rates by excitation of O$_2$, *Ann. Geophysicae*, **16**, 1007–1013, 1998c.

Pavlov, A. V., and A. A. Namgaladze, Vibrationally excited nitrogen in the upper atmosphere. Review paper (in Russian), *Geomagn. Aeron.*, **28**, 705–721, 1988.

Pavlov, A. V., and M. J. Buonsanto, Comparison of model electron densities and temperatures with Millstone Hill observations during undistributed periods and the geomagnetic storms of March 16–23 and April 6–12, 1990, *Ann. Geophysicae*, **15**, 327–344, 1997.

Pavlov, A. V., and K. A. Berrington, Cooling rate of thermal electrons by electron impact excitation of fine structure levels of atomic oxygen, *Ann. Geophysicae*, **17**, 1999 (in press).

Piper, L. G., The excitation of O(^{1}S) in the reaction between N$_2$(A$^3\Sigma_u^+$) and O(^{3}P), *J. Chem. Phys.*, **77**, 2372–2381, 1981.

Piper, L. G., Reevaluation of the transition- moment function and Einstein coefficients for the N$_2$(A$^3\Sigma_u^+$-X$^1\Sigma_g^+$) transition, *J. Chem. Phys.*, **99**, 3174–3181, 1993.

Prasad, S. S., and D. R. Furman, Electron cooling by molecular oxygen, *J. Geophys. Res.*, **78**, 6701–6707, 1973.

Prasad, J. S., J. S. Kim, and S. Okano, Observations of soft electron flux during SAR arc event, *Planet. Space. Sci.*, **28**, 375–379, 1980.

Radzig, A. A., and B. V. Smirnov, *The reference book in atomic and molecular physics* (in Russian), Atomizdat, Moscow, 1980.

Raitt, W. J., Schunk R. W., and P. M. Banks, Ionospheric composition in SAR-arcs, *Planet. Space Sci.*, **24**, 105–114, 1976.

Reed, E. I. and J. E. Blamont, Ogo 4 observations of the September 1967 M-arc, *EOS Trans. AGU*, **49**, 731, 1968.

Rees, M. H. and R. G. Roble, Observations and theory of the formation of stable auroral red arcs. *Rev. Geophys. Space Phys.*, **13**, 201–242, 1975.

Roble, R. G., and M. H. Rees, Time-dependent studies of the aurora: effects of particle precipitation on the dynamic morphology of ionospheric and atmospheric properties, *Planet. Space Sci.*, **25,** 991–1010, 1977.

Richards, P. G., An improved algorithm for determining neutral winds from the height of the F2 peak electron density, *J. Geophys. Res.*, **96,**17 839–17 846, 1991.

Richards, P. G., J. A. Fennelly, and D. G. Torr, EUVAC: a solar EUV flux model for aeronomical calculations, *J. Geophys. Res.*, **99,** 8981–8992, 1994. (Correction in *J. Geophys. Res.*, **99,** 13 283, 1994).

Robertson, A. G., M. T. Elford, R. W. Crompton, M. A. Morrison, W. Sun, and W.K. Trail, Rotational and vibrational excitation of nitrogen by electron impact, *Aust. J. Phys.*, **50,** 441–472, 1997.

Schmeltekopf, A. L., E. E. Ferguson, and F. C. Fehsenfeld, Afterglow studies of the reactions He^+, $He(2^3S)$, and O^+ with vibrationally excited N_2, *J. Chem. Phys.*, **48,** 2966–2973, 1968.

Schulz, G. J., A review of vibrational excitation of molecules by electron impact at low energies, in *Principles of laser plasmas*, Ed. G. Berkefi. Interscience, New York, 1976, p. 33–76.

Schunk, R. W., and A. F. Nagy, Electron temperatures in the F region of the ionosphere: Theory and observations, *Rev. Geophys. Space Phys.*, **16,** 355–399, 1978.

Shepherd, G. G., L. H. Brace, J. R. Burrows, J. H. Hoomann, H. G. James, D. M. Klumpar, A. F. Nagy, E. Stathopoulos, and J. H. Whitteker, An unusual SAR arc observed during ring current development, 4 August, 1972, *Planet. Space Sci.*, **28,** 69–84, 1980.

Singh, V., I. C. McDade, G. G. Shepherd, B. H. Solheim, W. E. Ward, The $O(^1S)$ dayglow emission as observed by the WIND imaging interferometer on the UAR, *Ann. Geophysicae*, **14,** 637–646, 1996.

Singhal, R. P., and A. E. S. Green, Spatial aspects of electron energy degradation in atomic oxygen, *J. Geophys. Res.*, **86,** 4776–4780, 1981.

Singhal, R. P., C. H. Jackman, and A. E. S. Green, Spatial aspects of low- and medium-energy electron degradation in N_2, *J. Geophys. Res.*, **85,** 1246–1254, 1979.

Slanger, T. G., and G. Black, $O(^1S)$ quenching by $O(^3P)$, *J. Chem. Phys.*, **64,** 3763–3773, 1976.

Slanger, T. G., B. J. Wood, and G. Black, The temperature dependence of $O(^1S)$ quenching by O_2, *Chem. Phys. Lett.*, **17,** 401–403, 1972.

Slater, D. W., C. Gurgiolo, J. U. Kozyra, E. W. Kleckner, and J. D. Winningham, A possible energy source to power stable auroral red arcs: precipitating electrons, *J. Geophys. Res.*, **92,** 4543–4552, 1987.

Stubbe, P., and W. S. Varnum, Electron energy transfer rates in the ionosphere, *Planet. Space Sci.*, **20,** 1121–1126, 1972.

Thomas, L. D. and R. K. Nisbet, Low-energy electron scattering by atomic oxygen, *Phys. Rev.*, **11,** 170–173, 1975.

Thomas, J. M., and F. Kaufman, Rate constant of the reactions of metastable $N_2(A^3\Sigma_u^+)$ in $v = 0, 1, 2$ and 3 with the ground state O and O_2, *J. Chem. Phys.*, **83,** 2900–2903, 1985.

Titheridge, J. E., Model results for the ionospheric E region: solar and seasonal changes, *Ann. Geophysicae*, **15,** 63–78, 1997.

Torr, M. R., and D. G. Torr, The role of metastable species in the thermosphere, *Rev. Geophys. Space Phys.*, **20,** 91–144, 1982.

Williams, J. F., and L. J. Allen, Low-energy elastic scattering of electrons from atomic oxygen, *J. Phys. B: At. Mol. Opt. Phys.*, **22,** 3529–3539, 1989.